

Three-dimensional simulations of the jet feedback mechanism in common envelope jets supernova

SHLOMI HILLEL,¹ RON SCHREIER,¹ AND NOAM SOKER¹

¹*Department of Physics, Technion, Haifa, 3200003, Israel;*
ronsr@technion.ac.il, shlomi.hillel@gmail.com, soker@physics.technion.ac.il

ABSTRACT

We conduct three-dimensional hydrodynamical simulations of common envelope jets supernova (CEJSN) events where we assume that a neutron star (NS) launches jets as it orbits inside the outer zones of a red supergiant (RSG) envelope, and find the negative jet feedback coefficient to be $\simeq 0.1 - 0.2$. This coefficient is the factor by which the jets reduce the mass accretion rate onto the NS as they remove mass from the envelope and inflate bubbles (cocoon). Our results suggest that in most CEJSN events the NS-RSG binary system experiences the grazing envelope evolution (GEE) before it enters a full common envelope evolution (CEE). We also find that the jets induce up and down flows in the RSG envelope. These flows together with the strong convection of RSG stars might imply that energy transport by convection in CEJSNe is very important. Because of limited numerical resources we do not include in the simulations the gravity of the NS, nor the accretion process, nor the jets launching process, and nor the gravity of the deformed envelope. Future numerical simulations of CEE with a NS/BH companion should include the accretion process onto the NS and vary the jets' power accordingly, the full gravitational interaction of the NS with the RSG, and energy transport by the strong convection.

Keywords: Supernovae — stars: jets — stars: variables: general — binaries: general

1. INTRODUCTION

In the common envelope jet supernova (CEJSN) scenario a neutron star (NS) or a black hole (BH), hereafter NS/BH, enters the envelope of a giant star, accretes mass through an accretion disk that launches jets, and spirals-in to the core of the giant star (e.g., Soker & Gilkis 2018; Gilkis et al. 2019; Soker et al. 2019; Grichener & Soker 2019a; López-Cámara et al. 2019, 2020; Soker 2021). The NS/BH spirals-in in this common envelope evolution (CEE), enters the core and further accretes mass from the core (for NS/BH merger with the core without explicitly including jets see, e.g., Fryer & Woosley 1998; Zhang & Fryer 2001; Barkov & Komisarov 2011; Thöne et al. 2011; Chevalier 2012; Schröder et al. 2020). Eventually the NS/BH tidally destroys the core such that the core material forms a massive accretion disk around the NS/BH. The interaction of the energetic jets that the NS/BH launches, in particular after it reaches the core, with the envelope leads to a bright transient event that can mimic a supernova. This is a CEJSN event. If the NS/BH accretes mass from the tenuous envelope to power a bright transient event but it does not spiral-in all the way to the core, the event is termed a CEJSN impostor (Gilkis et al. 2019).

There are two key processes that enable the CEJSN (or the CEJSN impostor) scenario. The first one is neutrino cooling that allows a very high mass accretion rate when the mass accretion rate is $\dot{M}_{\text{acc}} \gtrsim 10^{-3} M_{\odot} \text{ yr}^{-1}$ (Houck & Chevalier 1991; Chevalier 1993, 2012). The second process is that the NS/BH accretes mass through an accretion disc (e.g., Armitage & Livio 2000; Paphitis et al. 2015; Soker & Gilkis 2018). Different studies reach different values of the mass accretion rate (mainly whether it is close to the Bondi-Hoyle-Lyttleton [BHL] value of \dot{M}_{BHL} or whether it is much smaller), and on whether the accreted mass forms an accretion disk around the compact object (e.g., Rasio & Shapiro 1991; Fryer et al. 1996; Lombardi et al. 2006; Ricker & Taam 2008; Shiber et al. 2016; MacLeod & Ramirez-Ruiz 2015a,b; MacLeod et al. 2017). We will follow recent studies that show the formation of an accretion disk around the compact companion in a CEE (e.g., Chamandy et al. 2018), in particular for a NS companion (López-Cámara et al. 2020).

The case of NS/BH accretion is very different from cases of a main sequence star that spirals-in inside the envelope of a giant star. In particular relevant to our study are these two differences. (1) Main sequence stars have a hard time forming an accretion disk because of

their relatively large radius (e.g., Lopez-Camara et al. 2021 for recent simulations). NS/BH are much smaller and do not encounter this problem. (2) Main sequence star have difficulties in launching jets deep inside the envelope as the jets are choked (e.g., Lopez-Camara et al. 2021). The much deeper potential well of NS/BHs results in much more energetic jets that can expand to some distance in the envelope, even if they do not break out from the envelope (e.g., Grichener & Soker 2021). López-Cámara et al. (2019) and López-Cámara et al. (2020) find the NS companion in their CEE simulations to accrete at a rate of $\dot{M}_{\text{acc}} \approx 0.1 - 0.2\dot{M}_{\text{BHL}}$. We will consider even lower mass accretion rates in our study. We also note that the equation of state of the NS influences the outcome of accretion (e.g., Holgado et al. 2021).

The CEJSN scenario might account for some puzzling transient events and processes in astrophysics (e.g., Soker et al. 2019). Thöne et al. (2011) suggested that a merger of a NS and a helium star, which is known now as a CEJSN event, can account for the unusual Gamma-ray burst GRB 101225A. Soker & Gilkis (2018) proposed that the enigmatic supernova iPTF14hls (Arcavi et al. 2017) was a CEJSN event. The CEJSN might account also for SN 2020faa that is a similar supernova to iPTF14hls (see Yang et al. 2021 for the observations of SN 2020faa). Soker et al. (2019) proposed the CEJSN scenario for the fast-rising blue optical transient AT2018cow. The CEJSN might be one of the sites for the r-process nucleosynthesis (Papish et al. 2015; Grichener & Soker 2019a,b; Grichener, Kobayashi, & Soker 2022). As well, CEJSNe with BHs companions that launch the jets might be one of the sources of high-energy neutrinos (Grichener & Soker 2021). Based on these earlier studies Dong et al. (2021) suggested recently a CEJSN scenario for the luminous radio transient, VT J121001+495647.

Earlier studies found that jets in CEE with main sequence companions can remove a substantial amount of envelope mass when the main sequence is in the outer parts of the envelope (e.g., Shiber et al. 2019). This can increase the common envelope efficiency above unity, i.e., $\alpha_{\text{CE}} > 1$. Naturally NS/BH companions that launches jets can also bring the CEE efficiency to $\alpha_{\text{CE}} > 1$, as some scenario require for the CEE with a NS or a BH companion (e.g. Fragos et al. 2019; Zevin et al. 2021; García et al. 2021). In any case, our view is that jets that the NS/BH launches play a significant role in the CEE, and CEE simulations that involve a NS companion (e.g., Law-Smith et al. 2021) should eventually include jets to give a more accurate picture of the CEE.

Our main goal is to estimate the value of *negative jet feedback coefficient* in our simulations (section 5). This coefficient is the further reduction in the mass accretion rate because the jets inflate the envelope and eject mass, such that the density in the NS vicinity decreases. We do not calculate the full negative feedback cycle, but rather we follow the one-dimensional (1D) simulations of Grichener, Cohen, & Soker (2021) to estimate that coefficient, but now with 3D simulations.

We set the NS source of the jets to orbit inside the envelope of a red supergiant (RSG) star (section 2) and simulate several different cases (section 3). We do not include neither the self gravity of the envelope nor that of the NS. For detailed CEE simulations of a NS inside a RSG envelope that include these effects, but that do not include jets, see the recent studies by Lau et al. (2022) and Moreno et al. (2022). We also do not follow the accretion process. We preset the jets’ power and the orbital motion. As well, we set the jets to mix with the envelope mass in two cones about the equatorial plane, as we cannot resolve the launching zone of the jets (Schreier et al. 2021). These omissions allow us to follow the system for years, unlike simulations that include the accretion process onto the NS/BH and are therefore limited to evolution time of several days or less (e.g., Moreno Méndez et al. 2017; López-Cámara et al. 2019, 2020). To reach our goal we set the numerical scheme in a similar manner to earlier studies of jet-induced outflow in CEE (e.g., Shiber & Soker 2018; Schreier et al. 2019, but in the present study we include jets from a NS rather than from a main sequence star. We follow the flow structure in sections 4 and in section 5 we study the negative feedback process. We summarise our main results in section 6.

2. NUMERICAL SET UP

2.1. Basic simplifying assumptions

To facilitate long simulations, i.e., of several orbital periods, and to reach our goal of determining the negative jet feedback coefficient, we make the following basic assumptions.

2.1.1. A spherical star

We use the stellar evolution code MESA (Paxton et al. 2011, 2013, 2015, 2018, 2019) to evolve a zero-age-main-sequence star of $M_{1,\text{ZAMS}} = 15M_{\odot}$ for 1.1×10^6 yr, when it becomes a RSG star with a radius of $R_{\text{RSG}} = 881 R_{\odot}$, a mass of $M_1 = 12.5M_{\odot}$, metallicity of $Z = 0.02$, and an effective temperature of $T_{\text{eff}} = 3160K$. We take this RSG stellar model and install it at the center of our computational grid of the three-dimensional (3D) hydrodynamical code FLASH (Fryxell et al. 2000). The

density in the outer boundary of the initial RSG model is $\rho(R_{RSG}) = 2.1 \times 10^{-9} \text{ g cm}^{-3}$. The composition of the 3D star is pure hydrogen, and the code assume full ionisation. For numerical reasons we fill the initial numerical grid volume outside the star with gas of density $\rho_{\text{grid},0} = 2.1 \times 10^{-13} \text{ g cm}^{-3}$ and of temperature $T_{\text{grid},0} = 1100 \text{ K}$. We use this non-rotating spherical stellar model and neglect the process by which the NS spins-up the envelope before it enters the envelope.

2.1.2. A circular orbit

We simulate jets inside the envelope of a RSG star. We attribute these jets to a NS that orbits inside the envelope of the RSG star and accretes mass. We do not calculate the orbital in-spiral, and assume a circular orbit with a constant radius of $a = 700R_{\odot} = 0.79R_{RSG}$. We justify this simplifying assumption as our goals are to explore the flow structure in the envelope due solely to jets and to find the negative jet feedback coefficient. For the same reason we do not include the orbital energy that the NS releases as it spirals-in.

2.1.3. An inert inner core

To save expensive computational time we replace the inner 20% of the stellar radius, $R_{\text{in}} = 176 R_{\odot}$, with an inert ball having constant density, pressure, and temperature. We do include the gravitational potential of this inner inert ball.

2.1.4. A constant gravitational potential

The gravitational field in our simulation is constant in time and equals to that of the initial RSG star. Namely, we neglect both the gravity of the NS and of the deformed envelope. Again, the goal of this study is to explore the role of jets alone.

2.1.5. The jet-envelope interaction in the NS vicinity

The NS launches jets at $\approx 10^5 \text{ km s}^{-1}$. In addition, the NS is moving inside the envelope and we would like to resolve the entire RSG and its vicinity. Our computer resources do not allow us to resolve the region near the NS, and therefore we cannot accurately follow the early interaction of the jets with the envelope. To circumvent these difficulties we follow [Schreier et al. \(2021\)](#) and assume the following.

The NS launches very fast jets with a combined power of \dot{E}_{2j} . We take the jet-envelope interaction to occur inside two opposite lobes, each with a conical shape on opposite sides of the equatorial plane, with a combined volume of V_{2j} . The length of each lobe is $L_L = 7 \times 10^{12} \text{ cm}$ and its half opening angle is $\alpha_L = 30^\circ$. At the beginning of the time step the gas inside these cones has a total mass of $M_{2c,i}$, a total kinetic energy of $E_{2kc,i}$, and

a total thermal energy of $E_{2tc,i}$. We neglect the change in gravitational energy (as we neglect the self-gravity of the envelope) and the mass that the NS accretes from its vicinity and the mass that the jets add to the cones, as these are small in the specific simulations that we conduct.

The very fast jets that the NS launches carry a relatively low momentum. We assume that the momentum in the lobes is mainly due to the pressure gradient that the shocked jets build near the center. We further take the jet-envelope interaction near the NS to be like an explosion, and set the kinetic energy and the thermal energy after interaction to be equal to each other $E_{2kc} = E_{2tc}$. The velocity of the gas in the cones is radial of value $v_{c,r}$.

According to these assumptions then, the new properties of the gas inside the cones after jet-envelope interaction within a time step Δt are

$$\begin{aligned} M_{2c} &= M_{2c,i} \\ E_{2c} &= E_{2kc,i} + E_{2tc,i} + \dot{E}_{2j}\Delta t \\ E_{2kc} &= 0.5E_{2c}; \quad E_{2tc} = 0.5E_{2c}; \\ v_{c,r} &= \sqrt{2E_{2kc}/M_{2c}}, \end{aligned} \quad (1)$$

where the subscript ‘i’ refers to the beginning of the time step.

2.2. The computational scheme

2.2.1. The grid

The computational numerical grid is a cube with a side of L_G . The adaptive-mesh-refinement (AMR) of the numerical code FLASH divides to smaller cell sizes at zones of high gradients. We list the values of L_G and the sizes of the grid-cells for the different simulations in section 3. In the entire computational grid the equation of state of the gas is that of an ideal gas with an adiabatic index of $\gamma = 5/3$ plus radiation pressure. The centre of the RSG does not change and it is at $(x_1, y_1, z_1) = (0, 0, 0)$.

2.2.2. Accretion rates

We set the orbital motion of the source of the jets, the NS, to have a Keplerian circular orbit with a radius of $a = 700R_{\odot}$. The density of the unperturbed envelope at this radius is $\rho_0(700) = 7.9 \times 10^{-9} \text{ g cm}^{-3}$ and the mass of the giant star inner to this orbit is $M_1(700) = 11.3M_{\odot}$. The relative velocities of the NS and the envelope, neglecting envelope rotation, is $v_{\text{NS}}(700) = [G(M_{\text{NS}} + M_1(a))/a]^{1/2} = 59 \text{ km s}^{-1}$. The BHL accretion rate from the envelope

$$\dot{M}_{\text{BHL}} = \pi \rho(a) v_{\text{rel}}(a) \left[\frac{2GM_{\text{NS}}}{v_{\text{NS}}^2(a)} \right]^2 \quad (2)$$

in the unperturbed envelope for $a = 700R_{\odot}$ is

$$\dot{M}_{\text{BHL},0}(700) = 0.27M_{\odot} \text{ yr}^{-1}, \quad (3)$$

where we take for the NS mass $M_{\text{NS}} = 1.4M_{\odot}$ and subscript ‘0’ refers to the BHL accretion rate in the unperturbed envelope. For the relative velocity of the NS inside the envelope we take v_{NS} , although the velocity is somewhat lower due to envelope rotation. On the other hand, inclusion of the sound speed in the envelope reduces the accretion rate.

For the above mass accretion rate the gravitational accretion power is $\dot{E}_{\text{acc,BHL},0}(700) = 2.6 \times 10^{45} \text{ erg s}^{-1}$ for a NS with a radius of 12 km. We expect the power of the jets that the accretion disk launches to be

$$\dot{E}_{2j} = \zeta \dot{E}_{\text{acc,BHL},0} = \zeta \frac{GM_{\text{NS}} \dot{M}_{\text{BHL},0}}{R_{\text{NS}}}, \quad (4)$$

with $\zeta \approx 10^{-3} - 10^{-2}$ (Grichener, Cohen, & Soker 2021) because of the negative jet feedback mechanism (for a review see Soker 2016). Nonetheless, because of numerical limitations we will also simulate cases with much lower jets’ power. We return to the negative jet feedback mechanism in section 5.

3. SIMULATED CASES

We summarise the different simulations we conduct in Table 1. We list, from left to right, the name of the simulation, the combined power of the two jets, the ratio of this power to the unperturbed BHL accretion power ζ (equation 4), the full size of the numerical grid L_{G} , and the cell sizes. The presence of more than one size of cells is due to the AMR grid, with smaller cells in regions of high gradients. These sizes represent the resolutions of the numerical code. The first five columns are the input parameters of the simulations. In the sixth column we list the average factor by which the jets reduce the density in the envelope as we explain in section 5. We then list the figures in which we present the results from the respective simulations. The suffix ‘39’ in the name of RUN39 stands for the exponent of the jets’ power, and so forth. The Letter ‘L’ stands for the lowest resolution we use.

We did not simulate more powerful jets because of our limited computational resources. In reality, we expect the jets to be more powerful than the power we use in simulations RUN42L (section 5). However, with increasing jets’ power the flow velocities are higher and computational time becomes very long. In the cases of the high power simulations RUN41, RUN41L, and RUN42L we had to reduce the resolution. We cannot afford more powerful jets than in simulation RUN42L as then the much lower required numerical resolution would make the results unreliable.

4. THE FLOW STRUCTURE

We here present the flow structure that results from the jets. We recall that we do not include the spiralling-in of the NS to the envelope as we take a circular orbit at $a = 700R_{\odot}$. As well, we include neither the NS gravity nor the self gravity of the ejected mass. We do include the spherically-symmetric gravity of the RSG as it is when we start the simulation (it does not change with time). We also do not include initial envelope rotation that we expect due to the spiralling-in of the NS into the envelope. Our flow maps emphasise the role of the jets in ejecting the envelope.

Because we start with the NS already inside the envelope and the envelope is of an undisturbed RSG model, we must allow the binary system to have a relaxation time during which transient numerical features disappear. We find that this requires just over one orbital period of the NS. We therefore present the results only after two orbital periods $t = 2P_{\text{orb}} = 3.55 \text{ yr}$.

In Fig. 1 we present the density, temperature, and velocity maps of simulations RUN40 at $t = 2P_{\text{orb}} = 3.55 \text{ yr}$. At that time the NS is at $(x, y, z) = (49 \times 10^{12} \text{ cm}, 0, 0)$. The orbital plane is the $z = 0$ plane and the jets’ symmetry axis is perpendicular to the orbital plane and through the NS. In the left column we present these quantities in the plane $z = 6 \times 10^{12} \text{ cm} = 0.86L_{\text{L}}$, where L_{L} is the length of the cone into which we inject each lobe (section 2.1.5), and in the right column we present these quantities in the meridional plane $y = 0$ that contains the NS at that time.

The not-too-high jets’ energy of simulation RUN40 allows a large grid with a relatively high resolution (but still not sufficient to resolve the accretion process onto the NS). However, for the more realistic simulations RUN41, RUN41L, and RUN42L of higher jets’ powers we have to use a smaller grid and larger cells (lower resolution). For that we present in Fig. 1 the results of simulation RUN40. In Figs. 2 and 3 we present the flow of simulations RUN41L (left column) and RUN42L (right column). In Fig. 2 we present the density map in the plane $z = 0.86L_{\text{L}}$ (top panels), and in the $y = 0$ meridional plane (lower panels), while in Fig. 3 we present the velocity (upper panels) and temperature (lower panels) maps in the meridional plane $y = 0$. We present simulation RUN41L at $t = 2P_{\text{orb}}$. However, due to numerical difficulties we present simulation RUN42L at $t = 1P_{\text{orb}}$. We hope to overcome these numerical difficulties in the future.

First, we point out that we expect the jets in reality to be stronger than what our most energetic simulation RUN42L is (section 5). Nonetheless, we can learn the following from our simulations.

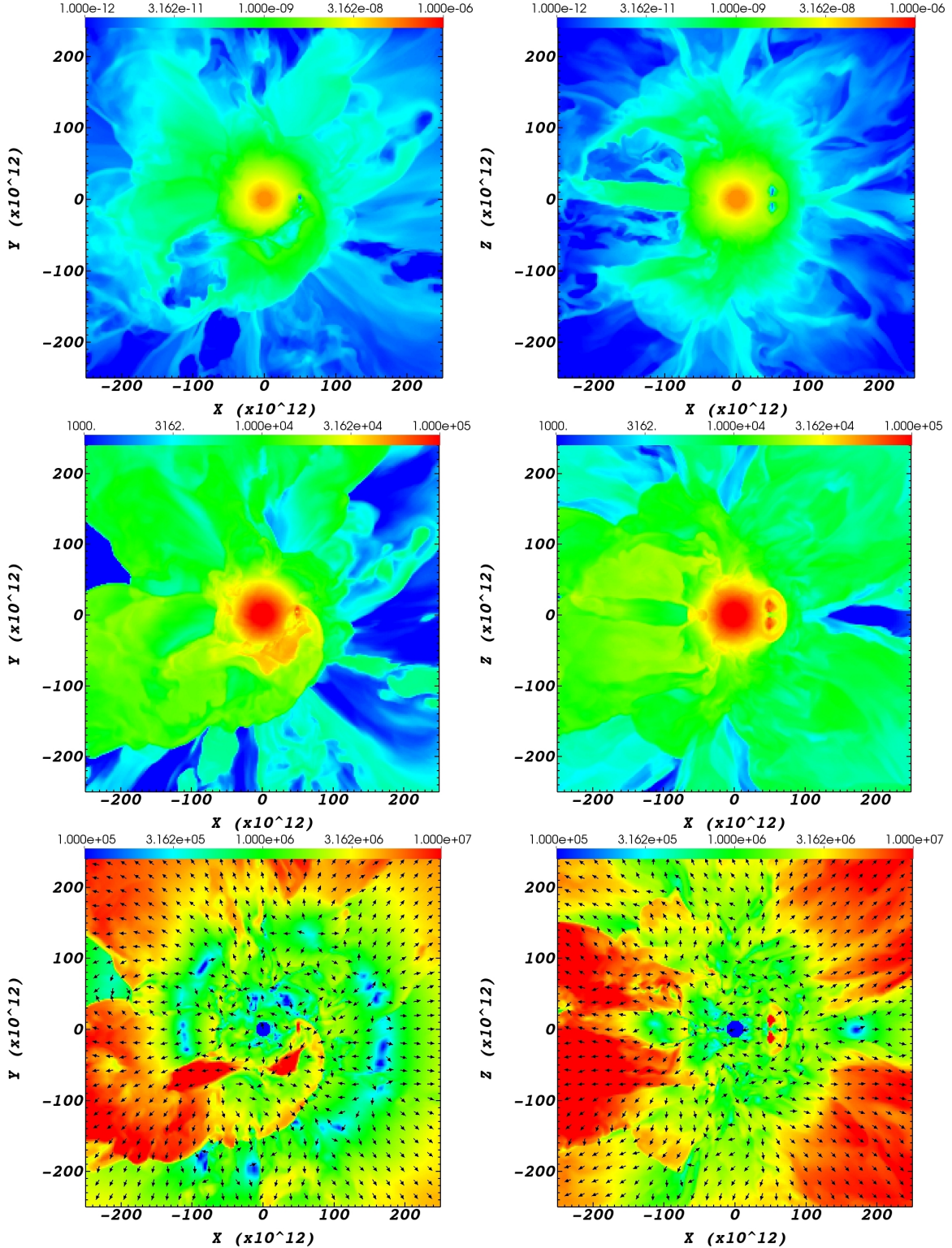


Figure 1. Results of simulation Run40 at $t = 2P_{\text{orb}} = 3.55$ yr. Left column: maps in the plane $z = 6 \times 10^{12}$ cm $= 0.86L_L$, where L_L is the length of the cone into which we inject each lobe, of the density (top panel; color bar from 10^{-12} g cm^{-3} to 10^{-6} g cm^{-3}), temperature (middle panel; color bar from 1000 K to 10^5 K) and velocity arrows on top of the velocity magnitude (bottom panel; color bar from 10^5 cm s^{-1} to 10^7 cm s^{-1}). Right column: similar maps but in the $y = 0$ meridional plane. The two cones into which we inject the jets' energy appear on the right panels at $x = a = 49 \times 10^{12}$ cm as two small regions on the two sides of the $z = 0$ plane, of low density (blue regions), high temperatures (red regions), and high velocity (red regions).

Run	\dot{E}_{2j} Jets' energy [erg s ⁻¹]	ζ Equation (4) [R_{\odot}]	L_G Grid Size [R_{\odot}]	Cell sizes Resolutions [R_{\odot}]	q_{ρ} Density decrease	Figures	comments
RUN39	3.16×10^{39}	10^{-6}	7184	56, 28, 14	0.8684	4, 5	
RUN40	3.16×10^{40}	10^{-5}	7184	56, 28	0.5248	1, 4,5	
RUN41	3.16×10^{41}	10^{-4}	3592	74.8, 37.4	0.4240	4,5	Medium resolution
RUN41L	3.16×10^{41}	10^{-4}	3592	112, 56	0.3011	2 - 5	
RUN42L	1.58×10^{42}	5×10^{-4}	3592	112, 56		2 - 4	Numerical difficulties

Table 1. The cases we simulate. In the second column we list the combined power of the two jets, and in the third column the value of ζ as we define in equation (4). We make use of the density reduction factor by jets q_{ρ} in section 5. Note that we could not finish simulation RUN42L. For other parameters see the text.

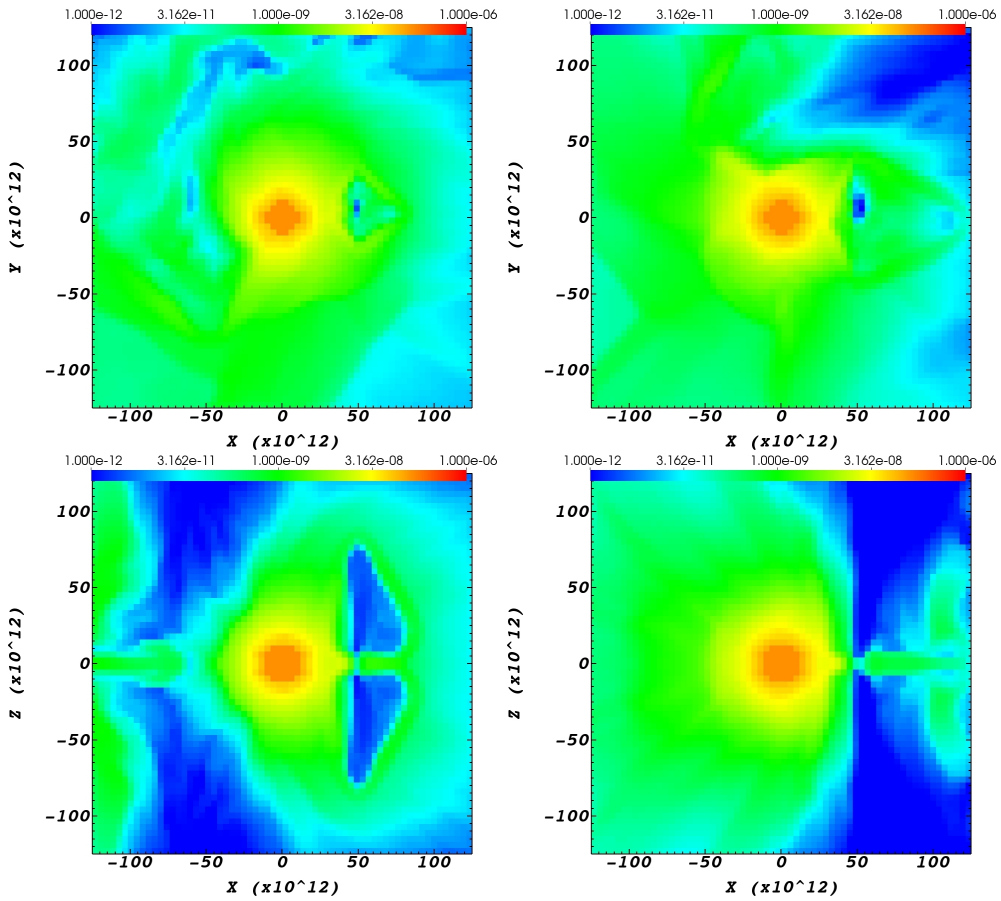


Figure 2. The density maps of simulations RUN41L (at $t = 2P_{\text{orb}}$; left column) and RUN42L (at $t = 1P_{\text{orb}}$; right column). In the upper panels we present the density maps in the plane $z = 0.86L_L$, and in the lower panels in the meridional plane $y = 0$ that contains the NS that is at $(x, y, z) = (49 \times 10^{12} \text{ cm}, 0, 0)$. Colour bars are from $10^{-12} \text{ g cm}^{-3}$ to $10^{-6} \text{ g cm}^{-3}$. The central square extending to $x = \pm 12 \times 10^{12}$ and $z = \pm 12 \times 10^{12}$ is the inert core of the simulation. It appears square and not circle because of the low numerical resolution. Note that much larger low density bubbles (cocoon) that the jets inflate relative to the case in Fig. 1.

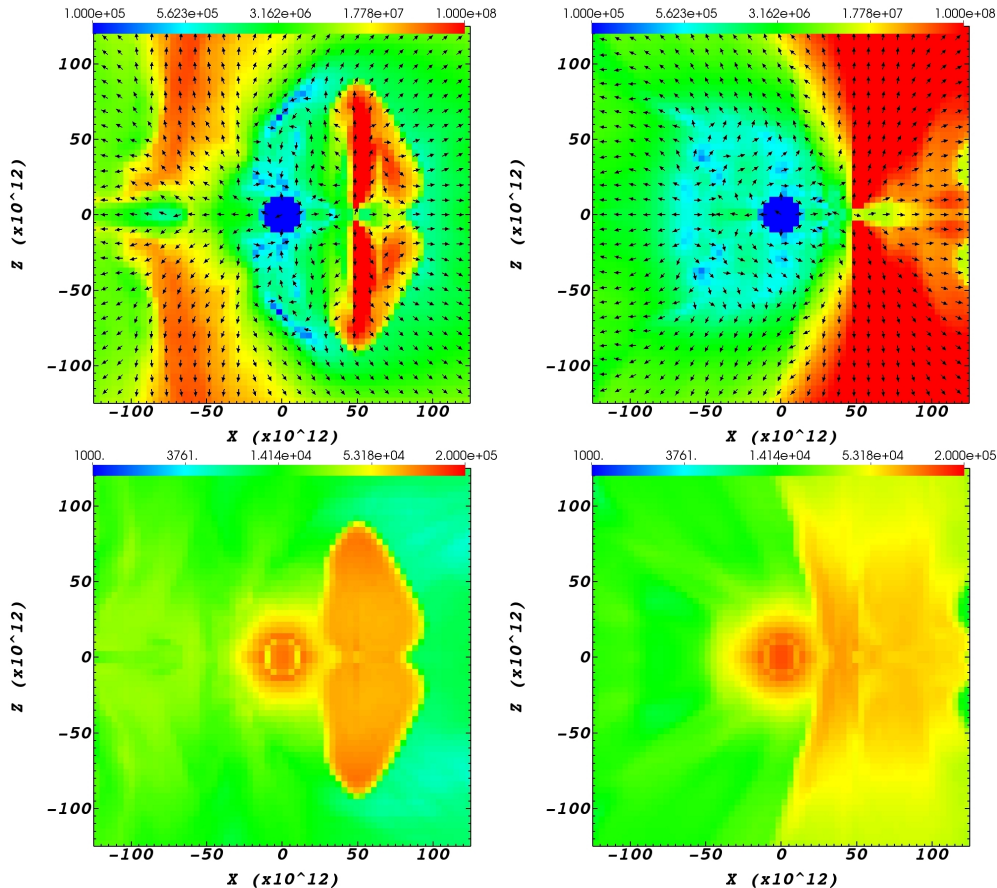


Figure 3. The velocity (upper panels; color bar from 10^5 cm s $^{-1}$ to 10^8 cm s $^{-1}$) and temperature (lower panels; color bar from 1000 K to 10^5 K) maps in the meridional plane $y = 0$ of simulations RUN41L (at $t = 2P_{\text{orb}}$; left column) and RUN42L (at $t = 1P_{\text{orb}}$; right column). Note that the velocity scale is an order of magnitude above that of Fig. 1.

1. *The grazing envelope evolution (GEE).* We find that for the low-energy simulations RUN39, RUN40 and RUN41L the jets do not break out from the envelope (i.e., choked jets). We see this as the blue lower density opposite zones where we inject the jets’ energy are surrounded by the dense envelope gas (in green; upper right panel of Fig. 1 and lower left panel of Fig. 2). In the more realistic simulation RUN42L the jets break out from the envelope and remove a very large portion of the outer envelope. Namely, the jets clean most of the envelope gas outside the orbit of the NS. If this holds for more realistic simulations that include more energetic jets and the spiralling-in process as well, then we would conclude that the NS-RSG binary system performs the GEE, at least while the NS is in the outer parts of the RSG (for hydrodynamical simulations of the GEE but with a main sequence companion rather than a NS companion see, e.g., Shiber 2018; Shiber et al. 2019; Lopez-Camara et al. 2021).

2. *Convection energy transport.* From the velocity maps (lower panels of Fig. 1 and upper panels of Fig. 3) we learn that the jets induce flow patterns that in-

clude inflow and outflow with respect to the center of the RSG (down-flow and up-flow). This flow pattern increases the down-flow and up-flow fluxes that already exist in the RSG envelope as a result of the strong convection. The convection in cool giants can be very efficient in transporting energy out, whether recombination energy or the energy that a companion deposits in the envelope during a CEE (e.g., Sabach et al. 2017; Grichener, Sabach, & Soker 2018; Wilson & Nordhaus 2019, 2020). We conclude that the flow that the jets induce in the envelope makes the convective energy transport more efficient even.

The main conclusions from this section to carry on to future numerical simulations of CEE with a NS/BH companion are that the simulations should include energy transport by convection (including the jet-induced down-flow and up-flow) and that researchers should be alert of the possibility of GEE at the beginning of the spiralling-in process in the envelope.

5. THE NEGATIVE JET FEEDBACK COEFFICIENT

We follow [Grichener, Cohen, & Soker \(2021\)](#) in finding the negative jet feedback coefficient χ_j , which is the factor by which the operation of the jets reduces the accretion rate. We take this value to be the factor by which the jets reduce the density along the NS orbit q_ρ , namely,

$$\chi_j = q_\rho \equiv \frac{\langle \bar{\rho}(t) \rangle}{\rho_0}, \quad (5)$$

where $\bar{\rho}(t)$ is computed as the average density over a thin spherical shell centred at the origin of the grid (centre of the RSG) and with a radius equal to the orbital radius of the NS, $\langle \bar{\rho}(t) \rangle$ is its time-averaged value, and ρ_0 is the density in the same region in the unperturbed envelope. We do not take the density within an accretion radius of the NS because we neglect the self gravity of the envelope and the NS's gravity, and because we do not follow the exact jet-envelope interaction. In [Fig. 4](#) we present the variation with time of $\bar{\rho}(t)$ for the different cases.

We calculate the time average $\langle \bar{\rho}(t) \rangle$ over the time that we present by the horizontal dashed black lines in [Fig. 4](#). We start the time averaging after the relaxation of the initial large perturbations. The density continues to fluctuate during the entire simulations, and so we average over few fluctuations. In the same way we calculate the value of ρ_0 , but in a simulation without jets (green line in [Fig. 4](#)). We list the values of q_ρ in the sixth column of [Table 1](#).

With the density reduction due to the jets the actual accretion rate onto the NS is then

$$\dot{M}_{\text{acc},j} = \chi_j \dot{M}_{\text{acc},0} = \chi_j \xi \dot{M}_{\text{BHL},0}, \quad (6)$$

where ξ is the ratio of the accretion rate to that of the analytical BHL value \dot{M}_{BHL} ([Hoyle & Lyttleton 1939](#); [Bondi & Hoyle 1944](#)). According to hydrodynamical simulations in most cases $\xi \simeq 0.1 - 0.5$ (e.g., [Livio et al. 1986](#) and [Ricker & Taam 2008](#) who did not include jets, and [Chamandy et al. 2018](#) who included jets), although some simulations deduce smaller values of $\xi < 0.1$ (e.g., [MacLeod & Ramirez-Ruiz 2015a](#); [MacLeod & Ramirez-Ruiz 2015b](#)).

The jets themselves carry a fraction of $\eta \simeq 0.1$ (down to 0.05) of the accretion power. Neutrino carry most of the accretion power as it is the neutrino cooling process that allows the high accretion rate. Overall, the power of the jets is according to equation (4) with

$$\zeta \equiv \eta \chi_j \xi \simeq 0.005 \chi_j - 0.05 \chi_j, \quad (7)$$

where in the second equality we substituted $\xi \eta \simeq 0.005 - 0.05$.

As for each simulation we predetermine the value of ζ ([Table 1](#)) and derive the density ratio q_ρ ([Table 1](#); beside

[Run42L](#)), by taking $\chi_j = q_\rho$ we can determine which value of χ_j fulfils equation (7). These simulations we consider to be self consistent according to the jet feedback mechanism and the values of $\eta \xi$ we adopt here. We cannot simulate high values of ζ because of numerical limitations. We therefore present in [Fig. 5](#) results for both our new 3D simulations (blue upper dots) and results from [Grichener, Cohen, & Soker \(2021\)](#) for their 1D simulations with a spiralling-in to orbital radius of 100 AU (lower red dots).

We manage to crudely fit the two sets of simulations with a line

$$\chi_j = -0.2 \log \zeta - 0.34. \quad (8)$$

Substituting equation (7) we obtain the equation for the negative jet feedback coefficient

$$5\chi_j + \log \chi_j = -\log(\eta \xi) - 1.7. \quad (9)$$

For $\eta \xi = 0.01$, $\eta \xi = 0.02$ and $\eta \xi = 0.05$, as examples, we obtain $\chi_j = 0.2$, $\chi_j = 0.16$, and $\chi_j = 0.11$ respectively. Overall, we find

$$\chi_j \simeq 0.1 - 0.2 \quad \text{for} \quad \eta \xi = 0.01 - 0.05. \quad (10)$$

Despite the uncertainties in the 1D simulations of [Grichener, Cohen, & Soker \(2021\)](#) and the uncertainties and density fluctuations in our new 3D simulations, we consider our estimate in equation (10) to be reasonable.

6. SUMMARY

We conducted 3D hydrodynamical simulations to further explore the role of jets in CEJSNs. In our numerical simulations we assumed that a NS companion orbits inside the outer envelope zones of a RSG star at a constant orbital radius of $a = 700 R_\odot$ and launches jets perpendicular to the orbital plane $z = 0$. We simulated 5 cases varying the power of the jets ([Table 1](#)). Due to the complicated flow structure with the energetic jets that NS companions launch we had to limit our numerical resolution and maximum jets' power. For numerical limitations and for our goal to reveal the role of jets, we did not include the gravity of the NS, nor the self gravity of the envelope, nor the spiralling-in process of the NS inside the RSG.

We emphasise that we expect that in most CEJSN events the jets be more energetic than the maximum power we could simulate in [RUN42L](#).

We present the flow structure after two orbital periods of simulation [RUN40](#) in [Fig. 1](#). This simulation has the most energetic jets that we could study with the high numerical resolution. In [Figs. 2](#) and [3](#) we present the results for the more energetic simulations [RUN41L](#) and [RUN42L](#), but that had low resolution (fifth column of [Table 1](#)).

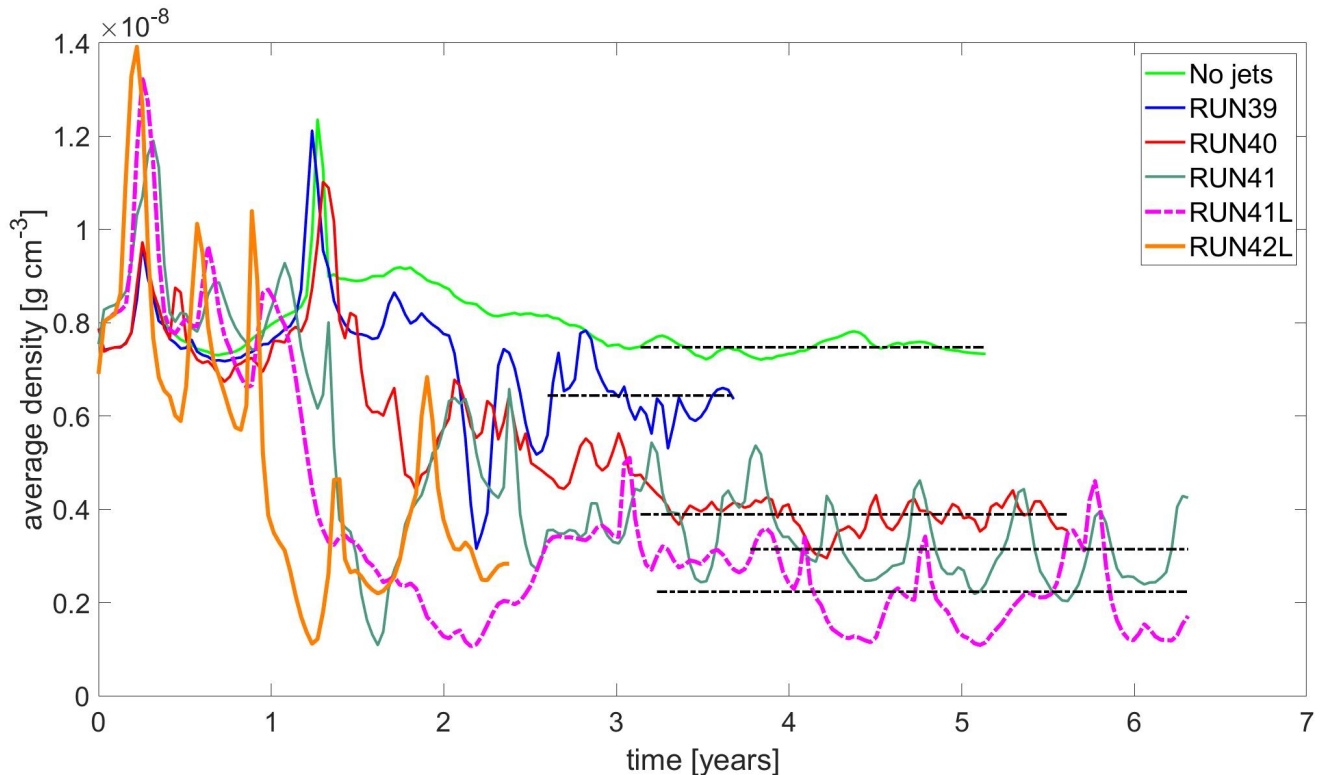


Figure 4. The average density $\bar{\rho}(t)$ over a thin spherical shell of radius $r = a = 700R_{\odot}$ as a function of time. The dashed horizontal line of each of five cases marks the time-averaged density $\langle \bar{\rho}(t) \rangle$ over a time periods as the dashed line marks.

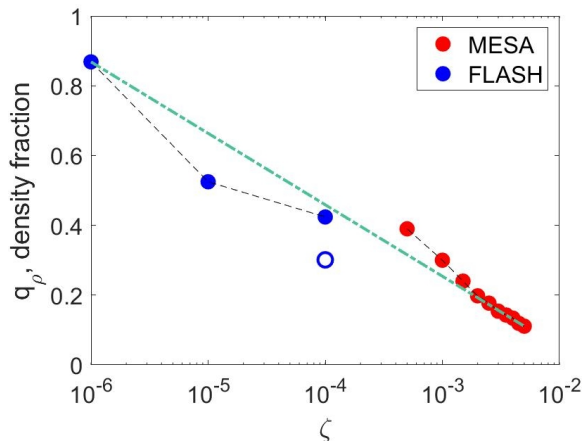


Figure 5. The magnitude of the jet feedback mechanism from the 1D simulations of Grichener, Cohen, & Soker (2021) (red dots) and our new 3D simulations in blue dots. The open blue-dot is of simulation RUN41L that is less reliable because of its lower resolution. The green dashed line is a fit through all the results according to equation 4.

From the flow structure we conclude the following (section 4). (1) In most CEJSN events we expect the NS-RSG binary system to experience the GEE before it enters a full CEE. (2) The jets induce down-flow and up-flow streams in the RSG envelope. These add to the already existing strong convection in the RSG envelope.

The stronger convection will be very efficient in transferring energy in the envelope (e.g., Grichener, Sabach, & Soker 2018; Wilson & Nordhaus 2020). Future numerical simulations of CEE with a NS/BH companion should include energy transport by the strong convection.

We calculated the average density of a thin spherical shell of radius $a = 700R_{\odot}$. This value fluctuates with time (Fig. 4). After the initial large fluctuations relaxed, we averaged the density over a time period that we mark by the horizontal dashed black lines on Fig. 4. We then calculated the factor q_{ρ} by which the jets reduce the average density (equation 5), and took this ratio to be the negative jet feedback coefficient χ_j . We list these values in the sixth column of Table 1. Because we could not simulate high-power jets, in Fig. 5 we connected the results of our 3D simulations with the 1D simulations of Grichener, Cohen, & Soker (2021). This allowed us to estimate the negative jet feedback coefficient that we give in equation (10). This is our main result.

Grichener, Cohen, & Soker (2021) estimated this range to be $0.04 - 0.3$. With the new simulations we narrowed somewhat this range to $\chi_j \simeq 0.1 - 0.2$. However, uncertainties are still large. Future simulations will have to better resolve the NS/BH vicinity, to include the gravity of the NS/BH, to include the self gravity of the

envelope, and most of all to include in the simulations the actual accretion rate onto the NS/BH and vary the jets' power accordingly.

ACKNOWLEDGMENTS

We thank Aldana Grichenr and Sagiv Shiber for helpful discussions. This research was supported by the Pazy Foundation.

REFERENCES

- Arcavi, I., Howell, D. A., Kasen, D., et al. 2017, *Nature*, 551, 210
- Armitage, P. J., & Livio, M. 2000, *ApJ*, 532, 540
- Barkov, M. V., & Komissarov, S. S. 2011, *MNRAS*, 415, 944
- Bondi, H., & Hoyle, F. 1944, *MNRAS*, 104, 273
- Chamandy, L., Frank, A., Blackman, E. G., et al. 2018, *MNRAS*, 480, 1898
- Chevalier, R. A. 1993, *ApJL*, 411, L33
- Chevalier, R. A. 2012, *ApJL*, 752, L2
- Dong D. Z., Hallinan G., Nakar E., Ho A. Y. Q., Hughes A. K., Hotokezaka K., Myers S. T., et al., 2021, *Sci*, 373, 1125. doi:10.1126/science.abg6037
- Fragos, T., Andrews, J. J., Ramirez-Ruiz, E., Meynet, G., Kalogera, V., Taam, R. E., & Zezas, A., 2019, *ApJL*, 883, L45. doi:10.3847/2041-8213/ab40d1
- Fryer, C. L., Benz, W., & Herant, M. 1996, *ApJ*, 460, 801
- Fryer, C. L., & Woosley, S. E. 1998, *ApJL*, 502, L9
- Fryxell, B., et al. 2000, *ApJS*, 131, 273
- García F., Simaz Bunzel A., Chaty S., Porter E., Chassande-Mottin E., 2021, *A&A*, 649, A114. doi:10.1051/0004-6361/202038357
- Gilkis, A., Soker, N., & Kashi, A. 2019, *MNRAS*, 482, 4233
- Grichenr A., Cohen C., Soker N., 2021, *ApJ*, 922, 61. doi:10.3847/1538-4357/ac23dd
- Grichenr A., Sabach E., Soker N., 2018, *MNRAS*, 478, 1818. doi:10.1093/mnras/sty1178
- Grichenr, A., & Soker, N. 2019b, *ApJ*, 878, 24
- Grichenr, A. & Soker, N. 2019b, arXiv:1909.06328
- Grichenr A., Soker N., 2021, *MNRAS*, 507, 1651. doi:10.1093/mnras/stab2233
- Grichenr, A., Kobayashi, C. & Soker, N. 2022, in preparation
- Holgado A. M., Silva H. O., Ricker P. M., Yunes N., 2021, *ApJL*, 910, L22. doi:10.3847/2041-8213/abecdd
- Houck, J. C., & Chevalier, R. A. 1991, *ApJ*, 376, 234
- Hoyle, F., & Lyttleton, R. A. 1939, *Proceedings of the Cambridge Philosophical Society*, 35, 405
- Lau M. Y. M., Hirai R., González-Bolívar M., Price D. J., De Marco O., Mandel I., 2022, arXiv:2111.00923
- Livio, M., Soker, N., de Kool, M., & Savonije, G. J., 1986, *MNRAS*, 222, 235. doi:10.1093/mnras/222.2.235
- Law-Smith, J. A. P., Everson, R. W., Ramirez-Ruiz, E., et al. 2021, arXiv:2011.06630
- Lombardi, J. C., Jr., Proulx, Z. F., Dooley, K. L., Theriault, E. M., Ivanova, N., & Rasio, F. A. 2006, *ApJ*, 640, 441
- López-Cámara, D., De Colle, F., & Moreno Méndez, E. 2019, *MNRAS*, 482, 3646
- Lopez-Camara D., De Colle F., Moreno Mendez E., Shiber S., Iaconi R., 2021, arXiv:2110.02227
- López-Cámara, D., Moreno Méndez, E., & De Colle, F. 2020, *MNRAS*, 497, 2057
- MacLeod, M., & Ramirez-Ruiz, E. 2015a, *ApJL*, 798, L19
- MacLeod, M., Antoni, A., Murguia-Berthier, A., Macias, P., & Ramirez-Ruiz, E. 2017, *ApJ*, 838, 56
- MacLeod, M., & Ramirez-Ruiz, E. 2015b, *ApJ*, 803, 41
- Moreno M. M., Schneider F. R. N., Roepke F. K., Ohlmann S. T., Pakmor R., Podsiadlowski P., Sand C., 2022, arXiv:2111.12112
- Moreno Méndez, E., López-Cámara, D., & De Colle, F. 2017, *MNRAS*, 470, 2929
- Papish, O., Soker, N., & Bukay, I. 2015, *MNRAS*, 449, 288
- Paxton, B., Bildsten, L., Dotter, A., et al. 2011, *ApJS*, 192, 3
- Paxton, B., Cantiello, M., Arras, P., et al. 2013, *ApJS*, 208, 4
- Paxton, B., Marchant, P., Schwab, J., et al. 2015, *ApJS*, 220, 15
- Paxton, B., Schwab, J., Bauer, E. B., et al. 2018, *ApJS*, 234, 34
- Paxton, B., Smolec, R., Schwab, J., et al. 2019, *ApJS*, 243, 10,
- Rasio, F. A., & Shapiro, S. L. 1991, *ApJ*, 377, 559
- Ricker, P. M., & Taam, R. E. 2008, *ApJL*, 672, L41
- Sabach E., Hillel S., Schreier R., Soker N., 2017, *MNRAS*, 472, 4361. doi:10.1093/mnras/stx2272
- Schreier R., Hillel S., Shiber S., Soker N., 2021, *MNRAS*, 508, 2386. doi:10.1093/mnras/stab2687
- Schreier, R., Hillel, S., & Soker, N. 2019, *MNRAS*, 490, 4748
- Schröder, S. L., MacLeod, M., Loeb, A., et al. 2020, *ApJ*, 892, 13
- Shiber S., 2018, *Galax*, 6, 96. doi:10.3390/galaxies6030096

- Shiber, S., Iaconi, R., De Marco, O., & Soker, N. 2019, MNRAS, 488, 5615. doi:10.1093/mnras/stz2013
- Shiber, S., Schreier, R., & Soker, N. 2016, RAA, 16, 117
- Shiber, S. & Soker, N. 2018, MNRAS, 477, 2584
- Soker, N. 2016, NewAR, 75, 1.
doi:10.1016/j.newar.2016.08.002
- Soker, N. 2021, MNRAS, 504, 5967.
doi:10.1093/mnras/stab1275
- Soker, N., & Gilkis, A. 2018, MNRAS, 475, 1198
- Soker, N., Grichener, A., & Gilkis, A. 2019, MNRAS, 484, 4972
- Thöne C. C., de Ugarte Postigo A., Fryer C. L., Page K. L., Gorosabel J., Aloy M. A., Perley D. A., et al., 2011, Natur, 480, 72. doi:10.1038/nature10611
- Wilson E. C., Nordhaus J., 2019, MNRAS, 485, 4492.
doi:10.1093/mnras/stz601
- Wilson E. C., Nordhaus J., 2020, MNRAS, 497, 1895.
doi:10.1093/mnras/staa2088
- Yang S., Sollerman J., Chen T.-W., Kool E. C., Lunnan R., Schulze S., Strotjohann N., et al., 2021, A&A, 646, A22.
doi:10.1051/0004-6361/202039440
- Zevin M., Bavera S. S., Berry C. P. L., Kalogera V., Fragos T., Marchant P., Rodriguez C. L., et al., 2021, ApJ, 910, 152. doi:10.3847/1538-4357/abe40e
- Zhang, W., & Fryer, C. L. 2001, ApJ, 550, 357